Spark Ignition of a Turbulent Shear-less Fuel-air Mixing Layer

Samer F. Ahmed[1,*] . Epaminondas Mastorakos[2]

1: Thermofluids Group, Department of Mechanical and Industrial Engineering, College of Engineering, Qatar University, P.O. Box 2713, Doha, Qatar

2: Engineering Department, University of Cambridge, Cambridge, CB2 1PZ, UK

Submitted to "Fuel Journal".

Original full-length research paper

Declaration:

This manuscript is unpublished material not being submitted for publication elsewhere

* Corresponding author

Dr. Samer F. Ahmed,

Department of Mechanical and Industrial Engineering

College of Engineering

Qatar University, P.O. Box 2713, Doha, Qatar

Tel : (974) 4403-4307

Fax : (974) 4403-4301

Email: sahmed@qu.edu.qa

Keywords: Spark ignition; Ignition probability; Turbulent mixing layer; Flame propagation.

Abstract

A planar methane-air mixing layer with equal velocity in the two streams has been used to examine the ignition probability and the non-premixed edge flame speed following spark ignition. The mixing layer has approximately homogeneous turbulent intensity and lengthscale. Mean local mixture fraction has also been measured for the whole flow field. The ignition and subsequent flame propagation were visualized with a high-speed camera and the flame's edges in the upstream, downstream and cross-stream directions have been identified. The average rate of flame evolution in these directions allowed an estimation of the average absolute flame speed. Ignition probability contour of the mixing layer takes a V-shape, which matches the shape of the lean and rich flammability limits with a little discrepancy in the rich side. By subtracting the uniform mean velocity resulted in estimates of the mean relative edge flame speed. This quantity was approximately $2.5S_L$, where S_L is the laminar burning velocity of stoichiometric methane-air premixed flames. The results are consistent with DNS of turbulent edge flames.

1. Introduction

Spark ignition of non-premixed combustion is important in high-altitude relight of aviation gas turbines, industrial furnaces, and some GDI automotive engines. Our physical understanding of such processes is not yet at a point that quantitative theoretical predictions can be made. Experiments with spark ignition of jet diffusion flames [1,2] showed that the probability of the emergence of an initial flame kernel in the spark neighbourhood is approximately equal to the probability of finding air-fuel mixture within the flammability limits. This concept has been further explored to provide a quantitative explosion risk

assessment [3] with CFD and a presumed shape of the PDF of the mixture fraction. Recently, spark ignition of non-premixed flames has been re-visited with jet [4], counter-flow [5], and bluff-body methane flames [6]. It was shown that, if ignition means the achievement of a full diffusion flame and not just the emergence of a small kernel that may be convected with the flow without causing flame ignition, the ignition probability is reduced and can be zero even in locations that have finite probability of flammable mixture fractions. The difference was attributed to local strain effects or high velocities that may not allow the flame kernel to grow or a flame to propagate, despite the local mixture fraction being flammable. This finding has been confirmed by studying the probabilistic nature of ignition of fully premixed turbulent flames in similar flow configurations [7] and in a swirled partially premixed burner [8]. It was noted that, in locations with high strain rates and/or high turbulence, these parameters have the detrimental effect on the ignition probability regardless of the mixture strength at these locations. In addition, the non-local effects, heat convection from the spark for instance, can play a very important part in determining the success of ignition [5], so that the ignition probability was finite even in regions of zero probability of finding flammable mixtures.

Simulations of spark ignition in a laminar non-premixed counterflow flame [9] reproduced these conjectures: ignition of the stoichiometric fluid could be achieved due to heat diffusion from the sparked region, even if that was located at rich or lean positions, and there was a critical strain rate, depending on the spark position and energy, above which ignition could not be achieved.

One additional reason why the ignition probability is less than unity, and why it is different than the probability of just establishing a small kernel, is that the flame cannot propagate against the flow to ignite the whole combustor. This, for example, has been

visualized in simple recirculating flames [7,10], but also in realistic gas turbine combustors [11-13]. Hence, to understand this problem better, the speed at which flames propagate in turbulent non-premixed reactants must be quantified. This propagation takes place, in principle, along the stoichiometric mixture fraction contour. When the mixture fraction fluctuates little about a nominally flammable value, so that it is always lean or always rich, premixed flame concepts can be used to describe flame propagation [14-16]. We may call this "stratified-charge premixed flame". When the mixture fraction fluctuates around the stoichiometric value, combustion occurs in a lean premixed, rich premixed, and non-premixed mode and the flame structure is reminiscent of so-called triple flames, which can merge under high strain rate to become edge flames [17]. Propagation of turbulent flames in this mode, which could be called "turbulent non-premixed edge flame", has not been studied well enough, although some relevant information has become available from studies on turbulent jet lifted flames [18,19]. In particular, from analyzing high-speed images of the flame at the stabilization height in jet flames [19], it has been concluded that the average edge flame speed is of the same order as the laminar burning velocity of the stoichiometric mixture S_L. The relative speed (i.e. flame edge speed relative to the fluid immediately ahead of the triple point) has been measured in the counterflow configuration [20] and its average value was around 0.75 S_L. Similar data from Direct Numerical Simulations of spark ignition and ensuing flame propagation in turbulent mixing layers in isotropic decaying turbulence [21-23] have revealed the detrimental effects of intense turbulence on absolute and relative edge flame propagation speed [21,22] and the effects of mixture fraction gradient and spark position on the structure and speed of the flame [23].

A detailed experiment study of spark ignition and flame propagation in the canonical problem of the turbulent mixing layer has not been performed yet. Hence, in this paper, we

present the characteristics of such a fuel-air mixing layer and we examine its ignition probability defined as the number of successful ignition events that result in a stable flame over the total number of spark attempts at certain location. In addition, the propagation speeds (relative to fixed coordinates) of the flame edge, as it expands along the layer have been measured. This propagation occurs against the flow on one side of the flame, with the flow on the other side, and against zero mean flow in the direction across the mean flow (parallel to the mixing layer). Hence the experiment allows various insights into edge flame propagation. The fact that the flow velocity is uniform facilitates an estimate of the average relative propagation speed. The experimental methods are presented next, while the results are presented and discussed in Section 3.

2. Experimental methods

2.1 Apparatus

The burner, Fig. 1, consists of two stainless steel channels with rectangular cross-section, whose two sides are W=46 mm and 20.5 mm, both being 500 mm long. The walls of the channels have a thickness of 2.5 mm. The two channels are attached along their length and their common wall is machined to produce a slope of 2.5 degrees, which results essentially in a splitter plate separating the two flows. At the edge of this plate (the exit of the channels), the height of each channel is H/2=23 mm. A quartz section of width W and height H is then fitted to provide optical access to the planar mixing layer formed downstream of the splitter plate between the flows in the two channels. A perforated plate with 40% solidity and holes of size M=3 mm to create turbulence is fitted 50 mm upstream of the splitter plate edge as shown in Fig. 1.

One channel of the burner carries air from the laboratory compressor and the other a fuel-air mixture. The fuel was methane (99.96% purity) and was mixed with 80% air (X=80%, by vol.). At this level of premixedness, the fuel-air stream is above the rich flammability limit and hence the flame formed between the two streams is of a non-premixed character. The air and fuel stream velocities at the exit were equal and, for most of the experiments reported here, the bulk velocities were U_b=3.0 m/s and, for some experiments, U_b=1.5 m/s. Both air and fuel flow rates were controlled by mass flow controllers. The Reynolds number of the flow in the channel before the perforated plate was 6720 (based on the hydraulic diameter).

The experiment has been designed in an effort to reproduce, at a smaller scale and adapted to the limitations imposed by safely performing a lab-scale combustion experiment, the shearless turbulent mixing layer studied experimentally by Ma and Warhaft [24]. It is also the experimental analogue of the DNS studied previously [21-23]. In particular, this experiment has turbulent Reynolds numbers close to those in the DNS, which facilitates some comparisons. To measure the streamwise (x) component of the velocity at various locations, a hot wire system was employed. A single constant-temperature Dantec 55P16 platinum-plated tungsten hot wire (diameter 5 μm and length 1.25 mm) was used with a DISA 55M01 standard bridge. The hot wire was placed perpendicular to the main flow direction and aligned with the z-direction. The measurements were taken with 10 kHz sampling rate and about 60,000 samples were recorded at each location using a DAQ system. The maximum statistical uncertainty for the reported mean velocities is estimated as 2%. All velocities reported are from the unignited condition.

2.2 Ignition unit

An ignition system was especially designed to produce repeatable sparks whose energy and duration could be varied independently. The main features of the unit can be found in Ref. [4]. The spark was created between two tungsten electrodes of 1 mm diameter, which were placed as shown in Fig. 1 to ensure minimum disturbance to the flow field. The electrodes had pointed edges to reduce the heat loss from the spark and the distance between them was 2 mm. The two electrodes were attached to a twin-bore ceramic tube, which was traversed axially and radially to cover the whole flow field with 0.1 mm resolution. For the experiments described here, the spark had duration of 400 μs and the electrical energy delivered by the circuit was 100 mJ. It should be mentioned that the repeatability of the spark energy produced from the ignition unit has been examined by using a Tektronics 6015A×1000 high voltage probe and an Ion Physics CM-1-L current transformer. Both devices have been connected to the spark electrodes and then the spark voltage and current waveforms have been detected by a Tektronics TDS 3012 digital oscilloscope with sampling rate of 1 MHz at the moment of spark. These waveforms have been presented in Refs. [4,25]. It was found that the maximum uncertainty of the spark energy produced from this ignition unit does not exceed 0.8% [25].

The ignition probability contour was measured by applying 50 single sparks at every chosen point. The number of successful ignition attempts that form a stable flame was divided by 50 to calculate the ignition probability at this location, which implies an uncertainty of 7.5% at 50% ignition probability [2]. For the current igniter configuration, about 30% of the spark energy is actually transferred to the combustible mixture [4]. This energy is much higher than the minimum ignition energy (6.41 mJ) required to ignite flammable methane–air mixtures under atmospheric conditions [26]. Each of the ignition

probability contours measured here was assembled from a matrix of 25 × 25 points across and along the burner.

2.3 High-speed imaging

The ignition events were monitored with a Phantom V4.2 Digital High Speed Camera fitted with a fast intensifier. A number of movies were captured with 4200 fps for successful and failed ignition events at different locations in the flow field in order to understand the behavior and the structure of the flame front from the moment of the spark until the establishment of the full planar turbulent flame or until blow-out of the domain. The images were imported to Matlab. For each image, a first stage of filtering removed noise, while a threshold was used at a second stage to detect the flame edge. This was done while traversing the domain from the clear area towards the flame zone. At this stage, each image includes black and white areas, with the white area represents the flame front. Therefore, the upstream, cross-stream and downstream flame edges were detected as a function of time for about 40 ms from the spark in each movie. A total of 40 such movies were made, from which average quantities were calculated. The estimated uncertainty of detecting the flame edge positions is about 1%.

2.4 Flame ionisation detector

The average mixture fraction has been measured by a CAMBUSTION HFR500 fast flame ionization detector (FID) with a 1 mm diameter sampling probe. The detector had a response time of about 0.9 ms and a sample gas flow rate of about 0.5 litre/min. The probe head and sampling line were heated at a temperature of 383 K. The probe was traversed

radially and axially with 1 mm steps. The spatial resolution of the probe can be determined from the sampling rate and the detection response. It is estimated at approximately 2 mm^3. The relative uncertainty due to calibration and detection with the FID is estimated at about 5%.

3. Results and discussion

3.1 Flame Visualization

Figure 1 shows photographs of the flame at a relatively low velocity, namely U_b=1.5m/s. At this velocity, the wake behind the splitter plate has low enough velocities to allow flame stabilization and hence, following ignition at a point downstream, the flame always propagates back towards the splitter plate to attach there. It is evident that the flame is planar and that the flame brush thickens downstream, probably due to the mixing layer growth.

Figure 2 shows snapshots during the flame evolution following a spark, with the flow at U_b=1.5m/s, a condition that leads to attached flames. The flame expands quickly in the downstream and the cross-stream directions (e.g. image at t=35.7 ms) and slowly propagates upstream against the incoming flow to eventually attach at the splitter plate (see image at t=178.5 ms). This cross-stream expansion has also been observed in the ignition of the annular combustor with multiple swirling injectors and it was described as “the volumetric expansion” [12,13]. The flame outline is clearly turbulent and quite sharp, which can lead to a determination of the flame edge. Figure 3 shows similar snapshots during the flame evolution at U_b=3.0 m/s, a condition that leads to flame growth but no stabilization. For this condition,

the downstream edge of the flame is convected out of the viewing window, as expected. The upstream edge is also being convected downstream, but at a slower rate than the downstream edge. In the cross-stream direction, the flame has filled the channel at a time that is somewhat earlier for the high velocity case than for the lower velocity case.

3.2 Velocity measurements

Figure 4 shows mean and r.m.s. velocities at various locations. The mean velocity is approximately uniform away from the splitter plate, but a thin wake immediately downstream of the splitter plate is evident. This wake region has low enough velocity (for the U_b=1.5m/s case) that flame propagation upstream and stabilization becomes possible. For the U_b=3.0m/s case, the mean velocity is larger, which prevents stabilization. As we go downstream, the mean velocity becomes uniform in the *y*- and *z*-directions.

The r.m.s. velocity is also quite uniform across the channel, even across the wake. At *x*=3 mm, u' is about 0.5 m/s (about 15% of the bulk velocity), decaying to about 0.25 m/s by *x*=83 mm. From measurements of the autocorrelation and using the Taylor hypothesis, the turbulent lengthscale was found to be approximately 7 mm at *x*=3 mm, growing to about 8 mm by *x*=83 mm. Detailed measurements of the mixture fraction will be presented in the next subsection to facilitate interpretation of the flame speed data.

3.3 Mixture fraction measurements

The mean fuel molar fraction has been measured for the whole flow field using Fast FID. These measurements have been obtained from a 2 sec sampling time of the probe at each location. Then, the mixture fraction has been calculated from these fuel molar fraction

measurements. Figure 5 shows three mixture fraction contours of the whole flow at different horizontal plans across the splitter. It should be mentioned that each mixture fraction contour has been plotted from a matrix of 80×40 measurement locations with 1 mm probe steps. It is evident that the mixture fraction distribution is very similar at z=0, z=15 and z=-15, which indicates the symmetry of the flow in z direction, Fig. 5 (a), (b) and (c) respectively. For the current air volume fraction in methane fuel, X=80%, the stoichiometric mixture fraction ξ_{st} is 0.452, while the lean and rich flammability limits are ξ_{lean} = 0.233 and ξ_{rich} = 0.732, respectively.

Figure 5 (a) shows the mixing field of the flow across the splitter at z=0 and along the burner with x direction. It can be observed that the mixing layer is not symmetric between the air side and the fuel side, as it is thicker into the fuel stream than the air stream. This may be related to different fluid properties, such as density and viscosity, that affect the mass diffusivities between the two streams. Therefore, the air is easier to diffuse into the fuel side than the fuel does in the air stream. In addition, it can be noted, in all the three contours shown in Fig. 5, that the 0.9 mixture fraction isoline makes a shift towards the left (away from the splitter plate) at about x=40 mm. It is not clear the reason behind this shift in the present investigation, but it can be related to the fact that the effect of the wake above the splitter is almost demolished above x=40mm, as shown in Fig. 4. This wake creates a small recirculation zone with about 5 mm width which restricts the diffusion mechanisms of the air towards the fuel side up to x=40 mm. This observation has been reported before in other investigations [27]. Above this location, more air diffuses that results in creating this shift in the fuel side. Moreover, the same reason can be also used to explain the relatively sudden increase in the distance between the other mixture faction isolines above x=40 mm. More

investigations are needed to fully clarify this point by using simultaneous PIV and acetone PLIF measurements that can be done in future research.

Figure 5 (a) also shows that the stoichiometric mixture fraction extends above the splitter in a thin layer with about 2 mm thickness. The lean flammability limit of the mixture fraction extends up to 5 mm in y-direction, while the rich one extends to about 10 mm close to the top of the burner. This makes the whole mixing layer thickness grows from about 5 mm at the tip of the splitter to about 15 mm thickness at the top of the burner as shown in Fig. 5 (a). Similar behavior can be observed in the other two contours at z=15 mm and z=-15 mm.

3.4 Ignition probability

The ignition probability has been measured for the whole flow field at U_b=3.0m/s. As mentioned early, successful ignition is the one that results in a fully stable flame, while any other case is considered to be a failed ignition. Figure 6 shows the ignition probability contour for this case with the lean and rich mixture fraction isolines. The ξ_{st} (not shown in the Fig.) locates in a thin layer along y=0, and it gets slightly wider as we moves with x direction as shown in Fig. 5. It can be observed from Fig. 6 that the ignition probability contour takes a V-shape with the region of the highest ignition probability locates around $\xi_{st.}$ This region becomes wider at the top of the burner following the same trend of ξ_{st}.

In y-direction, the ignition probability reduces sharply as moving away from the splitter, and the ignition is not possible at all beyond y=-2 mm at x=0 and y=-7 mm at x=80 mm in both the lean and the rich sides. Although the successful ignition limit matches the flammability limit in the lean side, the latter is wider than the successful ignition limit in the

rich side, Fig. 6. The ξ_{rich} extends up to y=11 mm at x=80 mm. This discrepancy between the ignition probability and ξ_{rich} can be attributed to the fact that the flame kernel is more likely to be convected downstream when ignition happens away from the splitter plan at y=0 mm, as observed from the high speed camera images in Fig. 3. The local flow velocity increases with y direction away from the splitter plan and reach a maximum values at y=±5 mm. Therefore, ignition beyond this location is more likely to be failed because the initial flame front propagation speed is obviously less than the local flow velocity, which results in flame propagation downstream rather than upstream. These results show that the local flow conditions have the detrimental effect on the success of ignition even in locations within the flammability limits. Similar conclusions have been obtained in the spark ignition of other flow configurations [4-7].

3.5 Edge flame velocity

Figure 7 shows schematically a typical flame outline following spark ignition at a point when the flow is at a velocity that does not permit upstream propagation and stabilization. The flame grows, as it is being convected downstream. The most upstream edge of the flame is denoted by X_u, the most downstream edge is denoted as X_d, the left-most edge by Z_l, and the right-most edge by Z_r. These quantities are extracted from each image from a sequence captured by the high speed camera.

Figure 8 shows examples of the time evolution of the flame edge location from ten separate ignition events. The average positions of X_u and X_d from 40 different ignition events, like those in dashed lines, are superimposed to produce the average flame edge locations versus

the time, shown in thick continuous lines in Fig. 8(a). Similarly, The average positions of Z_l and Z_r are shown in thick continuous lines in Fig. 8(b). Then, the edge flame speeds in all directions are obtained by calculating the slope of the average position curves (thick lines) against the time. It is evident that there is a shot-to-shot variation and that, during the evolution of the edge, its speed (understood as the slope of the curve with respect to time) is not constant. That is mainly due to the high turbulence intensity that ranges between 7 and 15% at different areas of flame propagation, as shown in Fig. 4. However, on average, the edge flame propagates along the same direction. This fact applies for all four directions of flame propagation studied here. Figure 8 shows that the downstream edge moves out of the domain after about 10 ms, while the upstream edge takes about 25 ms to be convected out of the imaged region. In the homogeneous *z*-direction, after about 2 ms the flame begins to expand at a relatively constant rate. The initial quick expansion due to the spark is evident by the fact that at about 0.5 ms from the initiation of the spark (t=0), the flame kernel has a diameter of about 4-5 mm.

Figure 9 shows the mean velocities of the flame after subtracting the mean velocity of the flow in the corresponding direction. This gives an estimate of the mean flame edge relative velocity. It is evident that: (i) differentiating the mean flame position results in a very noisy trace, especially for the streamwise direction; (ii) from between 4 to 10 ms, the relative speed is fluctuating less; and finally (iii) the two cross-stream directions give similar absolute speeds, as expected. To avoid the uncertainties associated with differentiating experimental data, linear fits have been performed to the mean edge flame positions (Fig. 10). So, an estimate of the downstream edge flame absolute speed ($d\langle X_d \rangle/dt$) is 4.53 m/s, giving an estimate of the downstream relative speed ($d\langle X_d \rangle/dt - U_b$) of 1.53 m/s; for the upstream edge, the mean absolute speed is $d\langle X_u \rangle/dt$ =2.1 m/s, giving a mean relative speed of $U_b - d\langle X_u \rangle/dt$

=0.9 m/s; while the two cross-stream velocities (d<Z_l>/dt and d<Z_r>/dt) are very close (0.99 and 1.0 m/s). There is no mean flow in the cross-stream direction. However, a cross-stream flow can be generated form the volumetric expansion across the flame [13]. Therefore, the absolute velocities that have been measured can serve as estimates of the relative velocity with reasonable accuracy.

It is clear that the mean relative edge flame speeds in the three directions (upstream and the two cross-stream) are approximately equal. For laminar edge flames, the estimate $(\rho_u/\rho_b)^{1/2}S_L$, where is the laminar burning velocity of the stroichiometric mixture, ρ_u the unburnt gas density and ρ_b the burnt-gas density, provides a good estimate of the absolute edge flame propagation speed in stagnant fluid [17]. For methane, S_L=0.4m/s and ρ_u/ρ_b =7.4 (for ambient conditions of reactants), which results in an edge flame speed of 1.1 m/s. Hence, for the present turbulent edge flame, the mean propagation speed is close to the result from laminar edge flames. This is fully consistent with DNS data [21], which provides credence to the present experimental measurements. In the downstream direction, the estimated relative speed is higher than this. This may be due to the expansion of the flow in the burnt region, which is expected to accelerate the mean flow in the streamwise direction. Note that the present estimates of flame speed are based on the mean flow velocity far from the flame edge, i.e. without taking the local flow expansion into account. When this expansion is taken into account, the flame edge relative to the flow velocity immediately ahead of the flame edge may be smaller than S_L, as found from experiments [20] and DNS [22].

4. Conclusions

A planar methane-air mixing layer with equal velocity in the two streams and approximately homogeneous turbulent intensity and lengthscale has been developed and used to examine flame speed following spark ignition. The flame propagation was visualized with a high-speed camera and the flame's edges in the upstream, downstream and cross-stream directions have been identified. The ignition probability of the whole flow field has been investigated and found that it takes a V-shape with the highest probability of ignition locates above the splitter plane. This shape matches the shape of the flammability limits of the mixture fraction with little deviation in the rich side. The ignition probability reduces sharply as moving away from the splitter plan. The average rate of flame evolution in all directions allowed for an estimation of the average absolute flame speed, while by subtracting the uniform mean velocity, estimates of the mean relative edge flame speed were made. The results show that this quantity was approximately 1 m/s, which corresponds to about 2.5 S_L. The results are consistent with DNS of turbulent non-premixed edge flames.

Acknowledgments

This work has been funded by the European Commission through project ``TIMECOP-AE" (AST5-CT-2006-030828). Thanks to Mr. I.A. Bahena Ledezma for assistance with the experimental techniques. S. F. Ahmed wishes to thank Qatar University for the support.

References

1. A. D. Birch, D. R. Brown, and M. G. Dodson. Ignition probabilities in turbulent mixing flows. Proceedings of the Combustion Institute, 18:1775-1780, 1981.

2. M. T. E. Smith, A. D. Birch, D. R. Brown, and M. Fairweather. Studies of ignition and flame propagation in turbulent jets of natural gas, propane and a gas with a high hydrogen content. Proceedings of the Combustion Institute, 21:1403-1408, 1986.

3. R. F. Alvani and M. Fairweather. Ignition characteristics of turbulent jet flows. Chemical Engineering Research and Design, 80:917-923, 2002.

4. S. F. Ahmed and E. Mastorakos. Spark ignition of lifted turbulent jet flames. Combustion and Flame, 146:215-231, 2006.

5. S. F. Ahmed, R. Balachandran, and E. Mastorakos. Measurements of ignition probability in turbulent non-premixed counterflow flames. Proceedings of the Combustion Institute, 31:1507-1513, 2007 .

6. S. F. Ahmed, R. Balachandran, T. Marchione, and E. Mastorakos. Spark ignition of turbulent non-premixed bluff-body flames. Combustion and Flame, 151:366-385, 2007.

7. S.F. Ahmed, The probabilistic nature of ignition in turbulent highly-strained lean premixed methane-air flames for low-emission engines, Fuel 134 (2014) 97-106.

8. L. Esclapez, E. Riber, B. Cuenot, Ignition probability of a partially premixed burner using LES, Proceedings of the Combustion Institute 35:3133–314, 2015.

9. E. S. Richardson and E. Mastorakos. Numerical investigation of forced ignition in laminar counterflow non-premixed methane-air flames. Combustion Science and Technology, 179:21-37, 2007.

10. M. Cordier, A. Vandel, G. Cabot, B. Renou, A.M. Boukhalfa, Laser-induced spark ignition of premixed confined swirled flames. Combustion Science and Technology 185 (2013) 379–407.
11. R. W. Read, J. W. Rogerson, and S. Hochgreb. Relight imaging at low temperature, low pressure conditions. AIAA Paper, pages AIAA-2008-0957, 2008.
12. M. Philip, M. Boileau, R. Vicquelin, E. Riber , T. Schmitt, B. Cuenot, D. Durox, S. Candel, Large Eddy Simulations of the ignition sequence of an annular multiple-injector combustor, Proceedings of the Combustion Institute 35:3159–3166, 2015.
13. J.-F. Bourgouin, D. Durox, T. Schuller, J. Beaunier, S. Candel, Ignition dynamics of an annular combustor equipped with multiple swirling injectors, Combustion and Flame 160:1398–1413, 2013.
14. T. Kang and D. C. Kyritsis. Methane flame propagation in compositionally stratified gases. Combustion Science and Technology, 177:2191-2210, 2005.
15. R. W. Bilger, S. B. Pope, K. N. C. Bray, and J. F. Driscoll. Paradigms in turbulent combustion research. Proceedings of the Combustion Institute, 30:21-42, 2005.
16. N. Pasquier, B. Lecordier, M. Trinite, and A. Cessou. An experimental investigation of flame propagation through a turbulent stratified mixture. Proceedings of the Combustion Institute, 31:1567-1574, 2007.
17. J. Buckmaster. Egde-flames and their stability. Combustion Science and Technology, 115:41-68, 1996.
18. K. M. Lyons. Toward an understanding of the stabilization mechanisms of lifted turbulent jet flames: Experiments. Progress in Energy and Combustion Science, 33:211-231, 2007.
19. A. Upatnieks, J.F. Driscoll, C.C. Rasmussen, S.L. Ceccio. Title. Combustion and Flame, 138:259-272, 2004.

20. C. Heeger, B. Böhm, S.F. Ahmed, R. Gordon, I. Boxx, W. Meier, A. Dreizler, E. Mastorakos. Statistics of Relative and Absolute Velocities of Turbulent Non-premixed Edge Flames Following Spark Ignition. To be presented at the 32nd International Symposium on Combustion, Montreal, August 2008.
21. N. Chakraborty, E. Mastorakos, and R. S. Cant. Effects of turbulence on spark ignition in inhomogeneous mixtures: a direct numerical simulation (DNS) study. Combustion Science and Technology, 179:293-317, 2007.
22. N. Chakraborty and E. Mastorakos. Numerical investigation of edge flame propagation characteristics in turbulent mixing layers. Physics of Fluids, 18:105103, 2006.
23. N. Chakraborty and E. Mastorakos. Direct numerical simulations of localised forced ignition in turbulent mixing layers: the effects of mixture fraction and its gradient. Flow, Turbulence and Combustion, 80:155-186, 2008.
24. B.K. Ma and Z. Warhaft. Some aspects of the thermal mixing layer in grid turbulence. Physics of Fluids, 29: 3114 -3120, 1986.
25. T. Marchione, S.F. Ahmed, E. Mastorakos. Ignition of turbulent swirling nheptane spray flames using single and multiple sparks. Combustion and Flame 156:166–80, 2009 .
26. B. Lewis, G.V. Elbe, Combustion, Flames and Explosions of Gases, Harcourt Brace Jovanovich, London, 1987.
27. J.A.T.A. Dantas, P.R. Pegoraro, J.A.W. Gut. Determination of the effective radial mass diffusivity in tubular reactors under non-Newtonian laminar flow using residence time distribution data. International Journal of Heat and Mass Transfer 71:18–25, 2014.

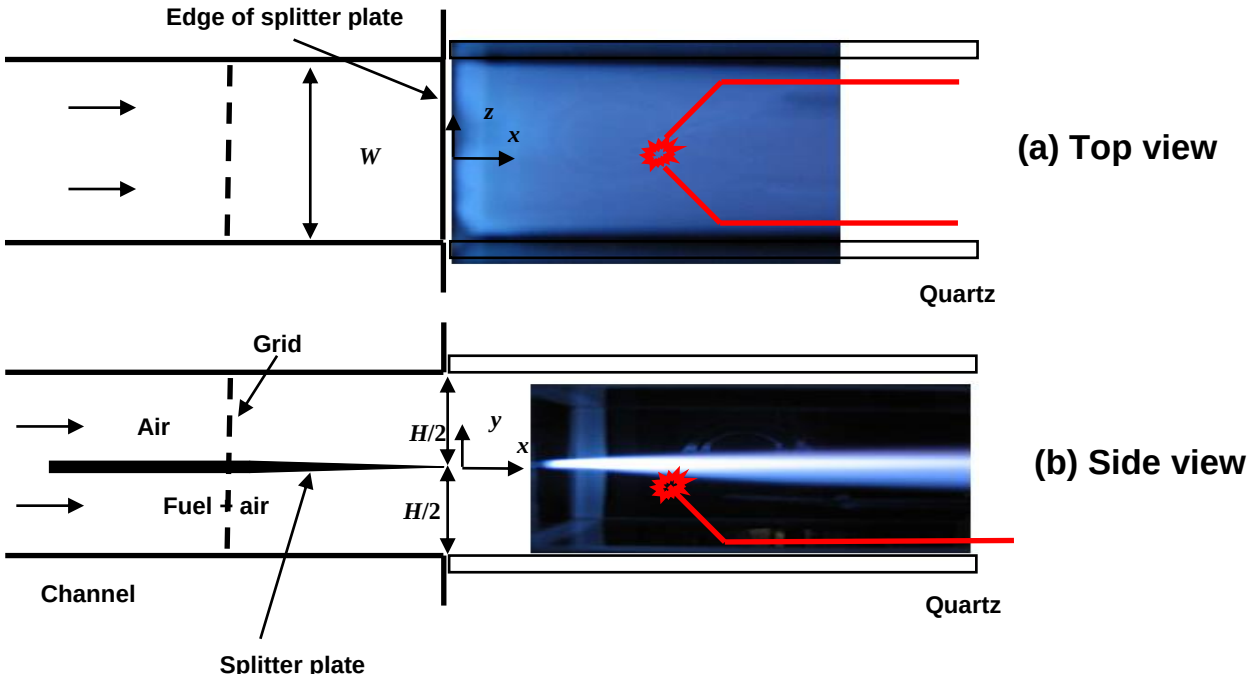

Figure 1. Schematic diagram of the test rig and photographs of the attached flame at U_b=1.5m/s. In the side view (b), the photo has been shifted to the right for clarity. The spark location and electrodes orientation is also shown by the thick red lines.

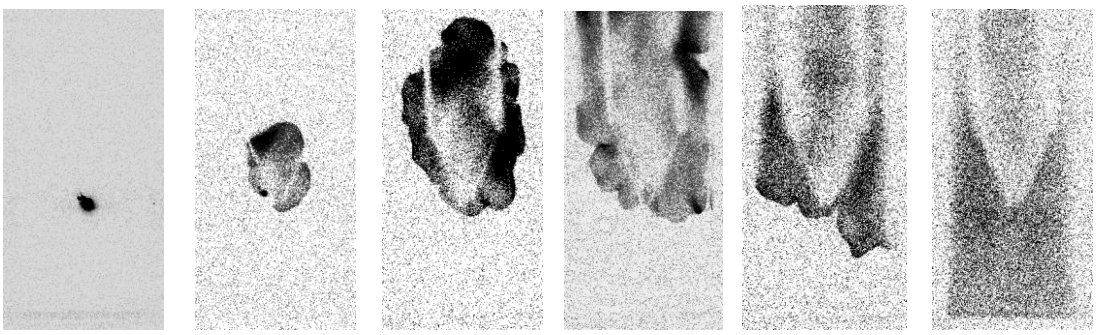

238 µs 11.9 ms 23.8 ms 35.7 ms 71.4 ms 178.5 ms

Figure. 2. Snapshots of flame following successful ignition at U_b =1.5m/s at different times after the spark. Top view (through the air stream), the flow comes from below. Camera settings: 4200 frames per second, exposure time: 228 µs. Image domain is 100x52 mm. The electrodes are visible due to the light emission from the flame. Spark at x=40mm, y=z=0.

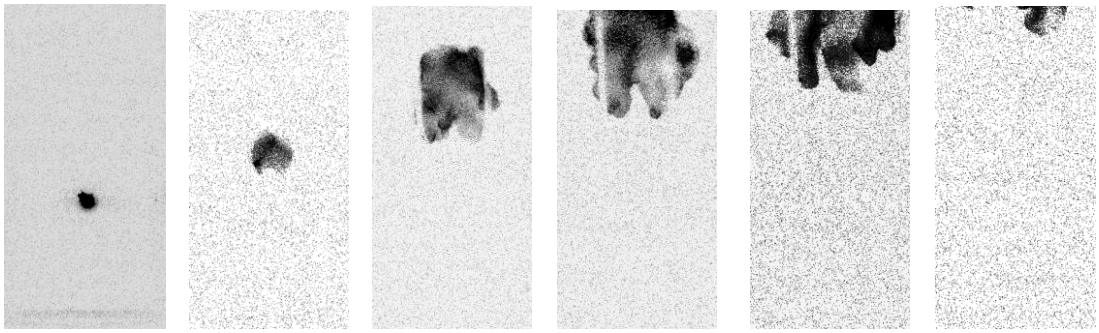

238 µs 5.9 ms 11.9 ms 17.8 ms 23.8 ms 35.7 ms

Figure 3. Snapshots of flame following failed ignition at U_b =3.0m/s at different times after the spark. All other parameters are as in Fig. 2.

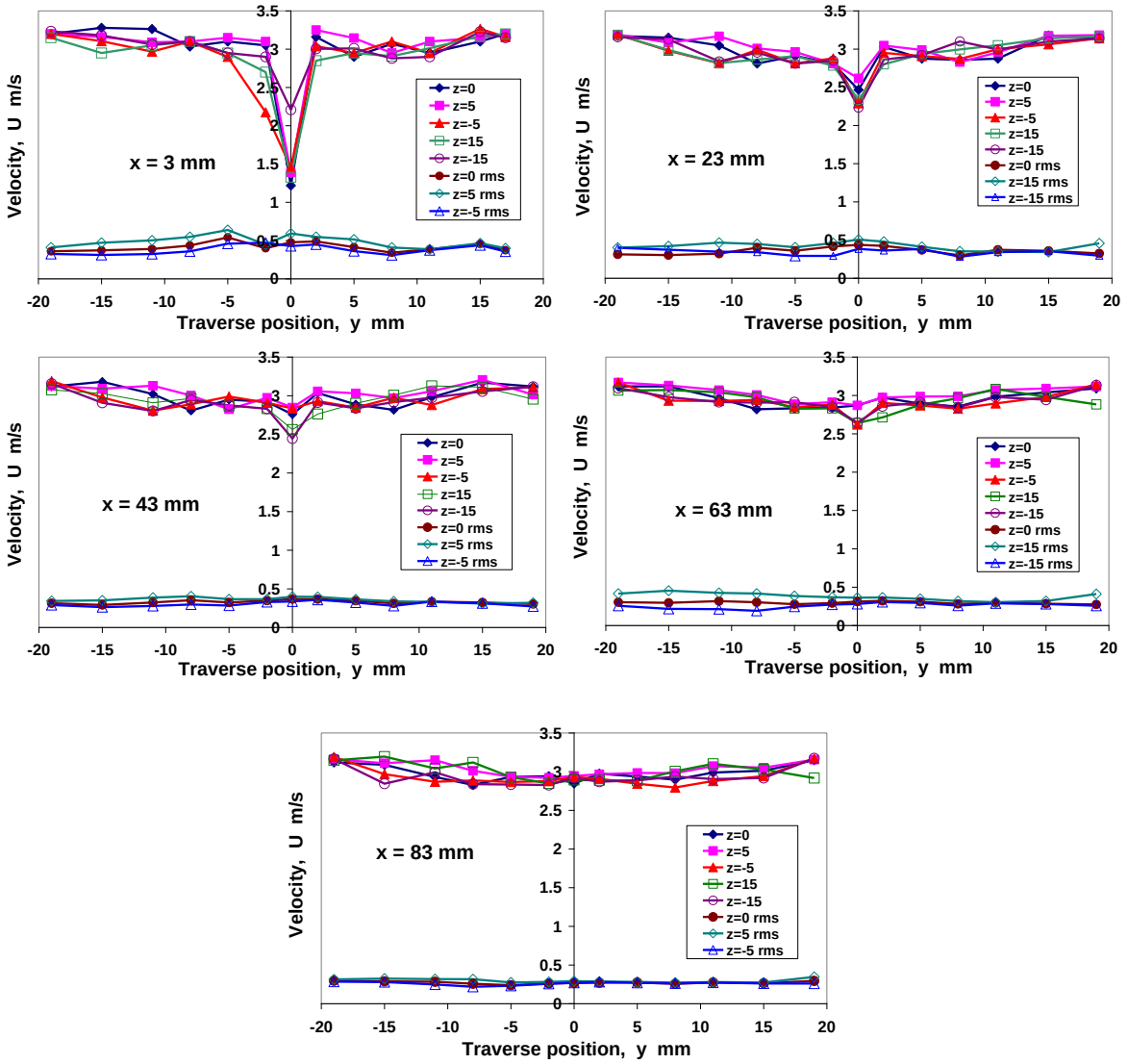

Figure 4. Mean and r.m.s. streamwise velocities at the indicated distance from the splitter plate edge. Flow condition: U_b =3.0 m/s.

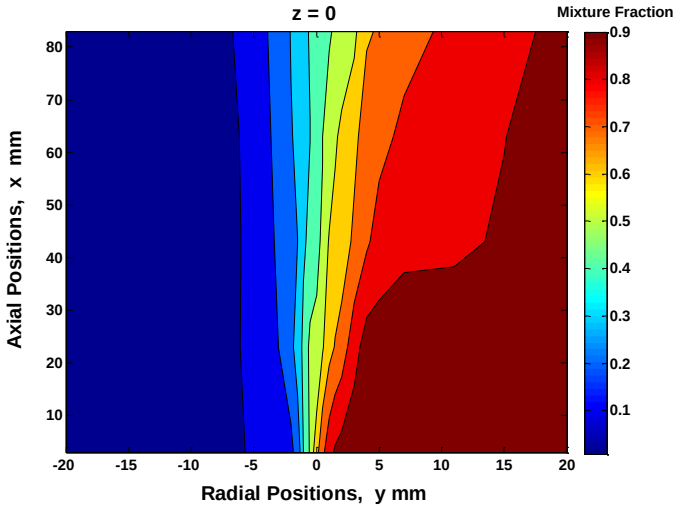

512

(a)

513

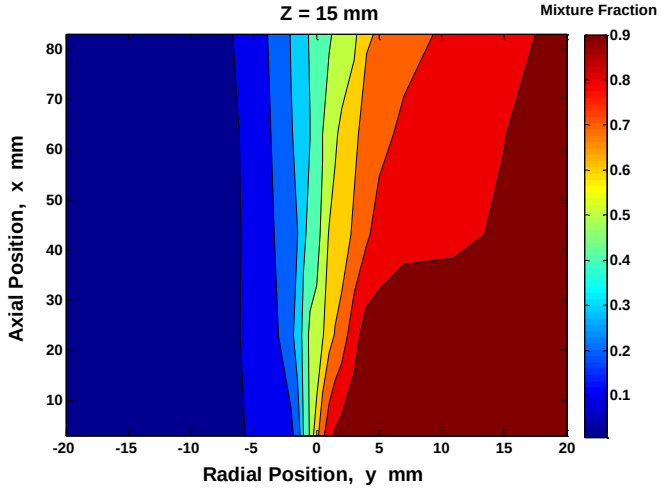

514

(b)

515

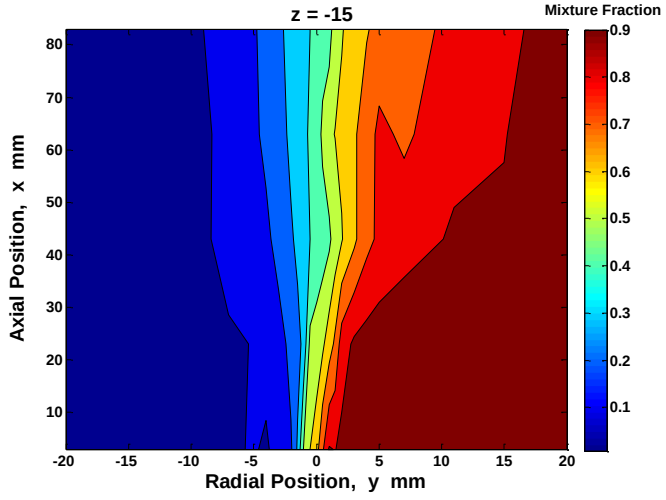

516

(c)

517

Figure 5. Mean mixture fraction measured by the FID at different radial plans across the splitter plate, (a) at z = 0; (b) at z = 15 mm; (c) at z = -15 mm. Flow condition: U_b =3.0 m/s and X=80%.

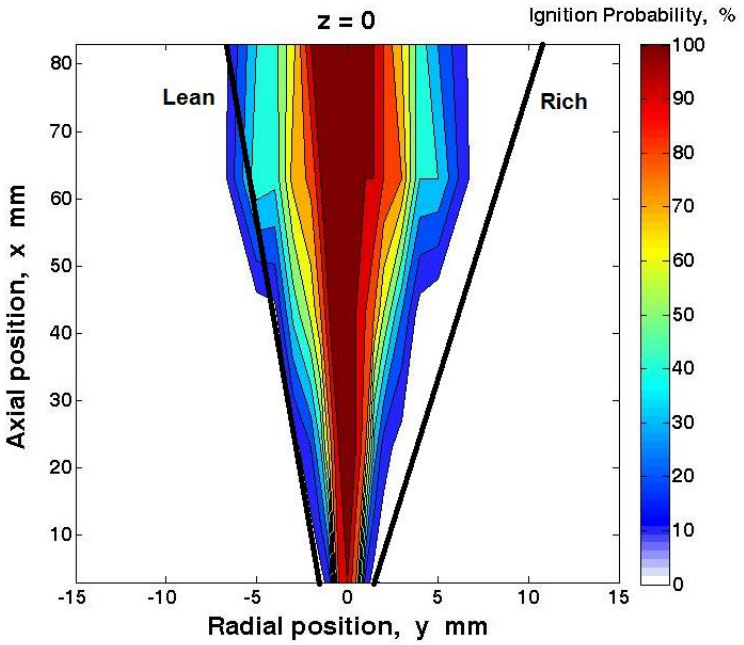

Figure 6. Ignition probability contour at z = 0. Lines indicate the lean and rich limits of mixture fraction, while stoichiometric mixture fracture isoline locates at y=0. Flow condition: U_b =3.0 m/s and X=80%.

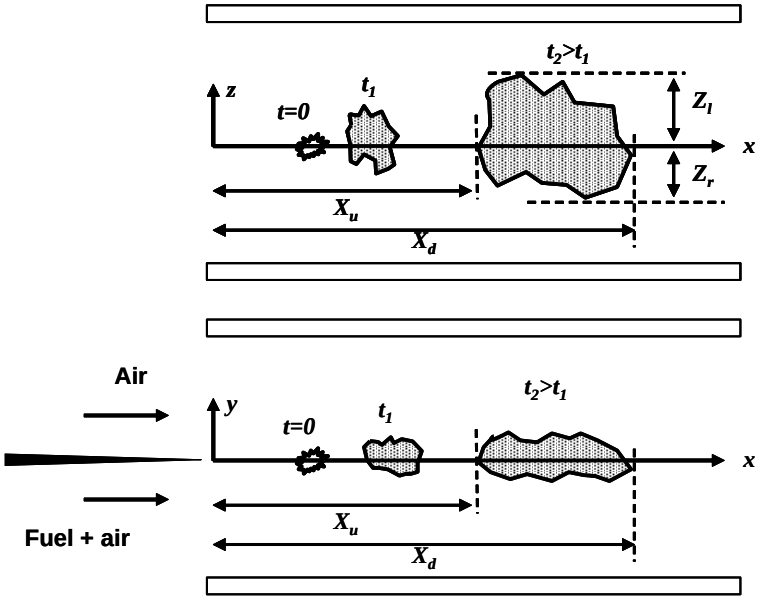

Figure 7. Sketch defining the edges of the flame from a top view of the expanding flame (as in Figs. 1a, 2 and 3) (upper sketch) and a side view (lower sketch). The flow comes from the left. The quantities X_u, X_d, Z_l, and Z_r are found as a function of time from each movie.

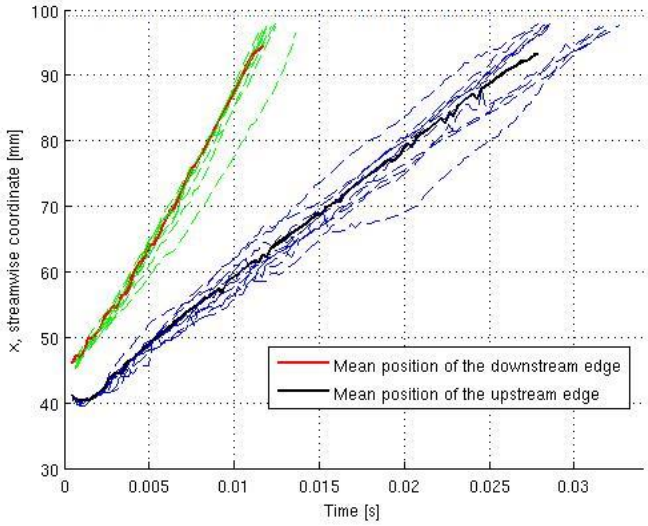

(a)

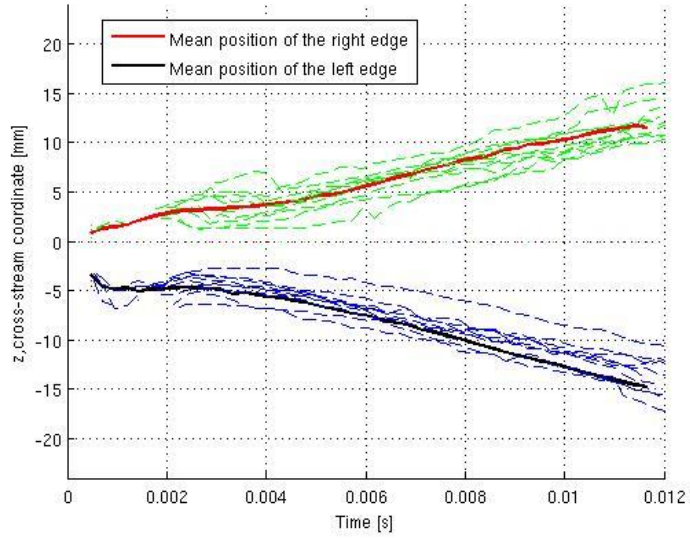

(b)

Figure 8. A few time evolutions of (a) X_u and X_d and (b) Z_l and Z_r from individual movies, denoted by dashed lines, and the corresponding averages compiled over 40 movies, denoted by thick lines. Flow conditions: U_b =3.0m/s and sparking at x =40mm, y=0, z =0.

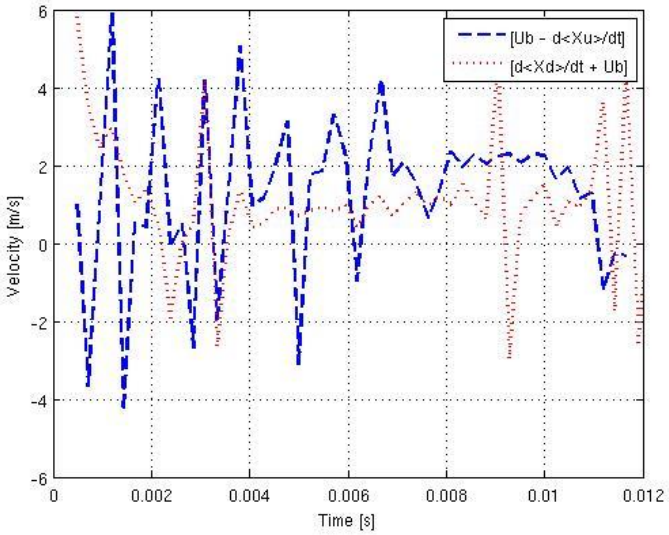

549

(a) 550

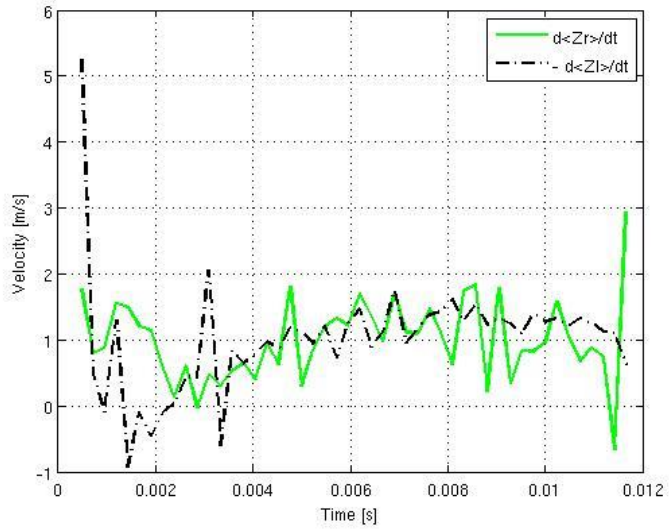

551

(b) 552

553

Figure 9. The time evolutions of (a) [U_b - d<X_u>/dt] and [d<X_d>/dt - U_b], and (b) d<Z_l>/dt 554
and d<Z_r>/dt. Flow conditions: U_b =3.0m/s and sparking at x=40mm, y=0, z=0. 555

556

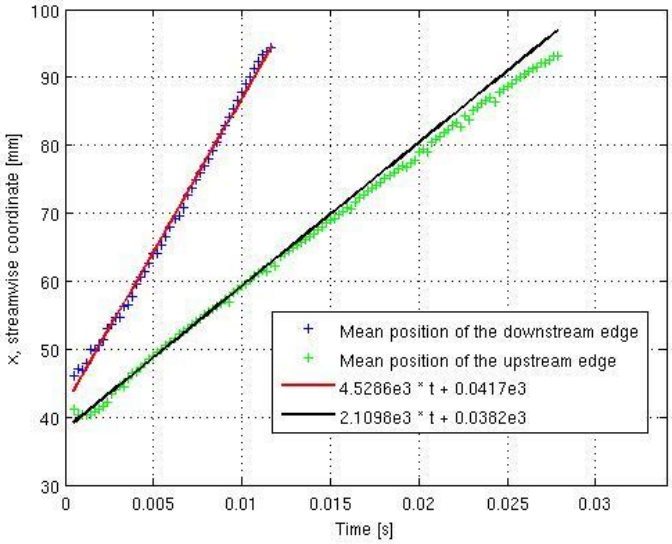

(a)

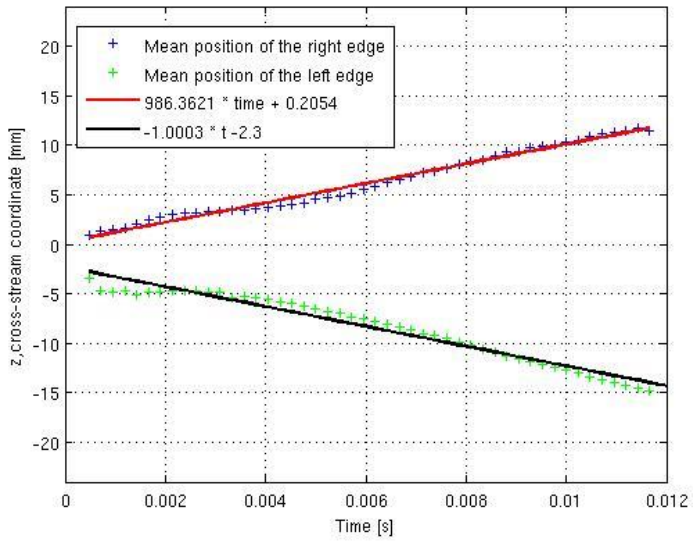

(b)

Figure 10. Linear curve fits to the mean flame edge position data of Fig. 8 (a) and (b), respectively.